terface resulted in CdSe thin films that remained crack-free during the deposition and annealing treatments. The surface structure of the treated substrates and the electrodeposited CdSe was clearly documented by SEM. The CdSe film morphology and structure was dependent on the method and conditions of the substrate preparation. The entire surface, inclusive of large features, was consistently covered by the CdSe, and no pinholes were evident. Upon annealing, no changes were evident in the structure or morphology of the CdSe. When removed from the substrate, the CdSe film remained crack-free. The CdSe surface, upon removal from the In/ITO or Cd/ITO substrates, showed shallow depressions where a portion of the interfacial material remained adherent to the substrate.

Preliminary resistivity measurements of CdSe showed that the substrate treatments not only affected the structure and adhesion of CdSe, but also the electrical properties. The CdSe samples from Se/ITO, after atmospheric exposure, gave consistent results. A more complete investigation of the effects of oxygen on the electrical properties of CdSe, and a more comprehensive study of the effects of Se, Cd, In, and other elements on the properties of CdSe are in progress.

Registry No. ITO, 50926-11-9; CdSe, 1306-24-7; Se, 7782-49-2; Cd, 7440-43-9; In, 7440-74-6.

Formation of Quantum-Size Semiconductor Particles in a Layered Metal Phosphonate Host Lattice

Guang Cao, L. K. Rabenberg,† Christine M. Nunn,‡ and Thomas E. Mallouk*

Department of Chemistry and Biochemistry, The University of Texas at Austin, Austin, Texas 78712-1167

Received July 25, 1990

Quantum-size ZnSe, PbS, CdS, and CdSe particles 30–50 Å in diameter were grown in the interlamellar region of the layered host material $Zr(O_3PCH_2CH_2CO_2H)_2$ by reaction of H_2S or H_2Se with $M^{II}[Zr(O_3PCH_2CH_2CO_2)_2]$. Diffraction from the PbS particles indicated the rocksalt structure, whereas CdSe adopts the zincblende structure and grows with the [111] zone axis parallel to the host layering direction. CdSe crystallites within a single host platelet are oriented relative to each other, even though the crystallinity of the host is destroyed during particle growth. Little or no reaction was found under similar conditions with $M^{II}[Zr(PO_4)_2]$. It is postulated that $M^{II}[Zr(O_3PCH_2CH_2CO_2)_2]$, prepared by dehydration of $M^{II}[Zr(O_3PCH_2CH_2CO_2)_2]\cdot xH_2O$ ($x \approx 1.4$) has an open structure that allows for interlamellar diffusion of H_2S and H_2Se. Contraction of the layer axis upon dehydration is significantly smaller for $M^{II}[Zr(O_3PCH_2CH_2CO_2)_2]\cdot xH_2O$ than for $M^{II}[Zr(PO_4)_2]\cdot yH_2O$. For comparison, an analogously layered compound, $Zn[Zn(O_3PCH_2CH_2CO_2)]_2\cdot 3H_2O$, was prepared and structurally characterized. This compound crystallizes in orthorhombic space group *Pbcn* (No. 60) with $a = 5.126$ (1), $b = 10.837$ (2), $c = 28.596$ (9) Å, $V = 1588.5$ Å^3, $Z = 4$, $R = 0.028$, $R_w = 0.033$ for 1567 unique reflections with $F_o > 3\sigma(F_o)$. The structure contains one set of zinc atoms four-coordinated by oxygen atoms of the phosphonate groups and another set five-coordinated by oxygen atoms of the carboxyl groups and lattice water molecules. The repeating unit is $Zn/O_3PCH_2CH_2CO_2/Zn(H_2O)_3/O_2CCH_2CH_2PO_3/Zn$... along the layering ($c$ axis) direction. Complete dehydration of this compound causes a relatively small decrease in the layer spacing, from 28.6 to 28.0 Å.

Introduction

There has been intense research activity in recent years on the subject of semiconductor crystallites that are so small (less than 100 Å in diameter) that they exhibit quantum size effects.[1] The interest in semiconductor particles in this size domain stems both from a desire to understand, at a fundamental level, the transition from molecular to bulk electronic properties and from the prospects of practical applications of these particles as nonlinear optical materials[2] and photocatalysts.[3]

Crystallites of nanometer sizes are inherently unstable due to their high surface tensions. Under conventional nucleation/growth conditions, crystallites tend to grow larger than the quantum size domain. Therefore without the use of stabilizing reagents and/or reactions, the preparation of small particles must take place under kinetically controlled conditions. In addition, even if crystallites of nanometer sizes are formed, they tend to aggregate or undergo Ostwald ripening to minimize their surface tension. In view of the factors affecting the size of crystallites it is not surprising to find that successful methods for the synthesis of nanoclusters always involve

† Department of Mechanical Engineering, The University of Texas at Austin, Austin, TX 78712-1167.

‡ Present address: University Chemical Laboratory, Lensfield Road, Cambridge CB2 1EW, England.

(1) For recent review articles, see: (a) Steigerwald, M. L.; Brus, L. E. *Annu. Rev. Mater. Sci.* **1989**, *19*, 471. (b) Henglein, A. *Top. Curr. Chem.* **1988**, *143*, 113. (c) Stucky, G. D.; Mac Dougall, J. E. *Science* **1990**, *247*, 669–678.

(2) (a) Wang, Y.; Suna, A.; Mahler, W. *Mater. Res. Soc. Symp. Proc.* **1988**, *109*, 187. (2) Wang, Y.; Mahler, W. *Opt. Commun.* **1987**, *61*, 233.

(3) (a) Youn, H.-C.; Tricot, Y.-M.; Fendler, J. H. *J. Phys. Chem.* **1987**, *91*, 581. (b) Kamat, P. V.; Dimitrijevic, N. M.; Fessenden, R. W. *J. Phys. Chem.* **1987**, *91*, 396. (c) White, J.-R.; Bard, A. J. *J. Phys. Chem.* **1985**, *89*, 1947. (d) Fojtic, A.; Weller, H.; Henglein, A. *Chem. Phys. Lett.* **1985**, *120*, 552. (e) Weller, H.; Fojtik, A.; Henglein, A. *Chem. Phys. Lett.* **1985**, *117*, 485.

(4) (a) Brus, L. *J. Phys. Chem.* **1986**, *90*, 2555. (b) Brus, L. E. *J. Chem. Phys.* **1984**, *80*(9), 4403. (c) Brus, L. E. *J. Chem. Phys.* **1983**, *79*(11), 5566.

(5) (a) Brus, L. E. *J. Chem. Phys.* **1983**, *79*, 5566. (b) Weller, H.; Schmidt, H. M.; Koch, U.; Fojtic, A.; Baral, S.; Henglein, A.; Kunath, W.; Weiss, K.; Dieman, E. *Chem. Phys. Lett.* **1986**, *124*, 557.

0897-4756/91/2803-0149$02.50/0

the use of terminating[6] or stabilizing[7] reagents and/or reactions and control of the diffusion of constituent chemicals with reagent concentration, reaction temperature, choice of reaction media, etc. One successful method for terminating and stabilizing quantum size clusters (Q particles) is the use of solid materials that control particle size by means of their microporous structure and that prevent Ostwald ripening by inhibiting molecular diffusion. Examples of this method include the formation of small CdS clusters within zeolite pores[8] and the formation of PbS or CdS Q particles of controllable sizes in polymeric ion-exchangers such as ethylenemethacrylic acid copolymers[9] and Nafion.[2,10] In the former case the cluster size is controlled by the pore size of the zeolite structure, and in the latter by varying the effective concentration of metal cation within the polymers prior to semiconductor cluster formation. A particularly interesting way of stabilizing Q particles is the formation of CdS clusters within Langmuir–Blodgett films;[11] this technique bears a resemblance to the present study in that Q particles are formed and stabilized within two-dimensional structures.

α-Zirconium phosphate, $Zr(HPO_4)_2 \cdot H_2O$, and its structural derivatives zirconium phosphonates, $Zr(O_3PR)_2$, have layered structures.[12] Layered compounds have seen very limited use as host matrices for the formation of semiconductor Q particles (only one example, the formation of CdS in clays, has been reported[13]). But as has been pointed out,[14] semiconductor Q particles formed with one strained dimension and two free dimensions are likely to be highly anisotropic, potentially giving rise to unusual photophysical properties. Morever, α-zirconium phosphate and phosphonates, being well ordered matrices, may exert a structural influence on the Q-particles formed within them. In this paper we report the results of an investigation of semiconductor Q-particle formation in layered zirconium phosphate and phosphonate hosts, and the crystal structure of a new layered zinc phosphonate $Zn[Zn(O_3PCH_2CH_2CO_2)]_2 \cdot 3H_2O$ to which the matrix compound $Zr(O_3PCH_2CH_2CO_2H)_2$ is structurally similar.

Experimental Section

Compound Synthesis. Chemicals were available from commercial sources and were used as received. α-Zirconium phosphate $Zr(HPO_4)_2 \cdot H_2O$ was prepared according to the literature procedure.[15] Zirconium bis(2-carboxyethylphosphonate) ($Zr(O_3PCH_2CH_2COOH)_2$) was also prepared as described in the literature,[16] with slight modification. Generally, 12.0 g of $ZrOCl_2 \cdot 8H_2O$ (37.3 mmol) dissolved in 50 mL of H_2O was mixed with 50 mL of an aqueous solution containing 4.8 g of 2-carboxyethylphosphonic acid (74.5 mmol) in a 250-mL plastic beaker. A white gelatinous precipitate formed immediately. While the mixture was stirred, a solution of 48% aqueous HF was slowly and carefully added so that the precipitate could be dissolved with a minimum amount of HF. (Fluoride ions form a stable complex with Zr^{4+}.) The clear solution so obtained was then kept at 60 °C and bubbled with nitrogen to slowly remove HF. After about 3–7 days the precipitation of microcrystalline $Zr(O_3PCH_2CH_2COOH)_2$ was complete. It was found that after the precipitate had appeared, addition of small amount of HF to partially dissolve the precipitate afforded platelike crystallites with a far more regular hexagonal appearance, as observed with transmission electron microscopy (TEM) (vide infra). The precipitate was filtered, washed with water until neutral, and dried at 70 °C in air. The composition was confirmed by elemental analysis, and the layer distance from X-ray diffraction (XRD) powder patterns (12.52 Å) was identical with that reported for this compound in the literature.[16]

Cations (Cd^{2+}, Pb^{2+}, or Zn^{2+}) were exchanged into the interlamellar region of α-zirconium phosphate or $Zr(O_3PCH_2CH_2COOH)_2$ by first converting α-zirconium phosphate into the n-butylamine intercalation compound,[17] and $Zr(O_3PCH_2CH_2COOH)_2$ into $Na_2[Zr(O_3PCH_2CH_2COO)_2] \cdot zH_2O$ by titration with NaOH. Then complete ion exchange was effected by contacting the n-butylamine intercalated α-zirconium phosphate or $Na_2[(O_3PCH_2CH_2COO)_2] \cdot zH_2O$ with 0.1 M aqueous solutions of $CdCl_2$, $ZnCl_2$, or $Pb(OAc)_2$ containing 1.2 equiv of the appropriate metal ions. After 36 h, the ion-exchange reactions were found to be over 97% complete by EDTA titration of the excess metal ions. Zn^{2+} and Cd^{2+} ions were directly titrated. The titration was done at pH 10.3 using an ammonium/ammonia buffer that contained trace amounts of Mg^{2+} for a sharper end point indication. Eriochrome black-T was used as indicator. Pb^{2+} was determined by using excess EDTA that was then back-titrated with Mg^{2+} by using Eriochrome black-T as indicator.[18] The layer spacings of $M^{II}[Zr(O_3PCH_2CH_2CO_2)_2] \cdot xH_2O$ (M = Cd, Pb, Zn) were apparent from their X-ray powder patterns and were the same (14.8 (1) Å) within experimental error, with little dependence on the lattice water content. The layer spacings of $M^{II}[Zr(PO_4)_2] \cdot yH_2O$, however, were variable depending on the drying conditions. When dried in air at 70 °C, the layer spacings were about 9.5 (3) Å. The water content of the ion-exchanged salts was determined by thermogravimetric analysis (TGA) measurements, and x, y, and z for $Cd[Zr(O_3PCH_2CH_2CO_2)_2] \cdot xH_2O$, $Cd[Zr(PO_4)_2] \cdot yH_2O$, and $Na_2[Zr(O_3PCH_2CH_2COO)_2] \cdot zH_2O$ were 1.366, 2.630, and 1.358, respectively. These samples were dried at 70 °C prior to analysis by TGA.

Preparation, Crystal Growth, and X-ray Crystal Structure of $Zn[Zn(O_3PCH_2CH_2CO_2)]_2 \cdot 3H_2O$. Single crystals were grown by first preparing 5 mL of an aqueous solution containing 0.1 M $ZnCl_2$, 0.06 M 2-carboxyethylphosphonic acid ($H_2O_3PCH_2CH_2COOH$), and 0.1 g of urea in a 10-mL vial. The clear solution was thermostated at 55 °C. After 1 week colorless crystals appeared at the bottom of the vial. A powder sample of this compound was prepared by simply combining aqueous solutions of zinc acetate and 2-carboxyethylphosphonic acid in the stoichiometric ratio. A white precipitate formed immediately. The product was isolated by filtration, washed with water, and dried in air at 50 °C. The composition of the product was confirmed by elemental analyses for C and H and by TGA determination of the lattice water content. The compound loses the three water molecules per formula unit in a single step (heating rate 20 °C/min) at temperatures from 90 to 170 °C under flowing nitrogen.

Data Collection. A colorless prismatic crystal having approximate dimensions 0.10 × 0.15 × 0.20 mm was mounted in a glass capillary with its long axis roughly parallel to the ϕ axis of the goniometer. Preliminary examination and data collection were performed with Mo Kα radiation (λ = 0.710 73 Å) on an Enraf-Nonius CAD4 computer-controlled κ-axis diffractometer equipped with a graphite crystal incident beam monochromator.

Cell constants and an orientation matrix for data collection were obtained from least-squares refinement, using the setting

(6) Herron, N.; Wang, Y.; Eckert, H. *J. Am. Chem. Soc.* **1990**, *112*, 1322.
(7) Kortan, A. R.; Hull, R.; Opila, R. L.; Bawendi, M. G.; Streigerwald, M. L.; Carrol, P. J.; Brus, L. E. *J. Am. Chem. Soc.* **1990**, *112*, 1327.
(8) (a) Herron, N.; Wang, Y.; Eddy, M. M.; Stucky, G. D.; Cox, D. E.; Moller, K.; Bein, T. *J. Am. Chem. Soc.* **1989**, *111*, 530. (b) Moller, K.; Bein, T.; Herron, N.; Mahler, W.; Wang, Y. *Inorg. Chem.* **1989**, *28*, 2914. (c) Wang, Y.; Herron, N. *J. Phys. Chem.* **1987**, *91*, 257.
(9) (a) Mahler, W. *Inorg. Chem.* **1988**, *27*, 435. (b) Wang, Y.; Suna, A.; Mahler, W.; Kasowski, R. *J. Chem. Phys.* **1987**, *87*(12), 7315.
(10) Smotkin, E. S.; Brown, R. M., Jr.; Rabenberg, L. K.; Salomon, K.; Bard, A. J.; Campion, A.; Fox, M. A.; Mallouk, T. E.; Webber, S. E.; White, J. M. *J. Phys. Chem.*, in press.
(11) Smotkin, E. S.; Lee, C.; Bard, A. J.; Campion, A.; Fox, M. A.; Mallouk, T. E.; Webber, S. E.; White, J. M. *Chem. Phys. Lett.* **1988**, *152*, 265.
(12) Clearfield, A. *Chem. Rev.* **1988**, *88*(1), 125.
(13) (a) Liu, X.; Thomas, J. K. *J. Colloid Surf. Sci.* **1989**, *129*, 476. (b) Stramel, R. D.; Nakamura, T.; Thomas, J. K. *Chem. Phys. Lett.* **1986**, *130*, 423.
(14) Thomas, J. K. *J. Phys. Chem.* **1987**, *91*, 267.
(15) Alberti, G.; Torracca, E. *J. Inorg. Nucl. Chem.* **1967**, *30*, 317.
(16) Dines, M. B.; DiGiacomo, P. M. *Inorg. Chem.* **1981**, *20*, 92.
(17) Peng, G.-Z.; Clearfield, A. *J. Inclusion Phenom.* **1988**, *6*, 49.
(18) (a) Ayers, G. H. *Quantative Chemical Analysis*, 2nd ed.; Harper & Row: New York; p 617. (b) Welcher, F. J. *The Analytical Use of Ethylenediaminetetraacetic Acid*; Van Nostrand: New York, 1958; pp 103–146.

angles of 21 reflections in the range $12 \leq \theta \leq 16$, measured by the computer-controlled diagonal slit method of centering. The instrument, refinement, and crystal data are listed in Table S1 (supplementary material; see the paragraph at the end of the paper).

From the systematic absences $hk0$, $h + k = 2n$; $h0l$, $l = 2n$; $0kl$, $k = 2n$; and from subsequent least-squares refinement, the space group was determined to be *Pbcn* (No. 60).

Intensity data were collected at a temperature of 24 (1) °C using the ω–2θ scan technique. The scan rate varied from 1 to 10°/min (in ω). The variable scan rate allows rapid data collection for intense reflections where a fast scan rate is used and ensures good counting statistics for weak reflections where a slow scan rate is used. Data were collected to a maximum 2θ of 60.0°. The scan range (in degrees) was determined as a function of θ to correct for the separation of K doublet;[19] the scan width was calculated as follows:

$$\text{scan width} = 0.7 + 0.350 \tan \theta$$

Moving-crystal moving-counter background counts were made by scanning an additional 25% above and below this range. Thus the ratio of peak counting time to background counting time was 2:1. The counter aperture was also adjusted as a function of θ. The horizontal aperture width ranged from 4.0 to 4.6 mm; the vertical aperture was set at 4.0 mm. The diameter of the incident beam collimator was 0.7 mm and the crystal-to-detector distance was 21 cm. For intense reflections an attenuator was automatically inserted in front of the detector, the attentuation factor was 21.0.

Data Reduction. A total of 2720 reflections were collected, of which 2311 were unique and not systematically absent. As a check on crystal and electronic stability, two representative reflections were measured every 60 min. The intensities of these standards remained constant within experimental error throughout data collection. No decay correction was applied.

Lorentz and polarization corrections were applied to the data. The linear absorption coefficient is 48.7 cm^{-1} for Mo Kα radiation. An empirical absorption correction based on a series of ψ scans was applied to the data. Relative transmission coefficients ranged from 0.686 to 0.997 with an average value of 0.890. An extinction correction was not necessary.

Structure Solution and Refinement. The structure was solved by using the Patterson heavy-atom method, which revealed the position of the two Zn atoms. The remaining atoms were located in succeeding difference Fourier maps. Hydrogen atoms were located, and their positions and isotropic thermal parameters were refined. The structure was refined in full-matrix least-squares analysis, and the weight w is defined as $4|F_o/(F_o)|$.

The standard deviation of the structure factors, $\sigma(F_o)$, is defined as follows:

$$\sigma(F_o) = [S(C + RB) + (p|F_o|)]/Lp$$

where S is the scan rate, C is the total integrated peak count, R is the ratio of scan time to background counting time, B is the total background count, Lp is the Lorentz–polarization factor, and the parameter p is a factor introduced to downweight intense reflections. Here p was set to 0.050.

Scattering factors were taken from Cromer and Weber.[20] Anomalous dispersion effects were included in F_c;[21] the values for f' and f'' were those of Cromer.[22] Only the 1567 reflections having intensities greater than 3.0 times their standard deviation were used in the refinements. The final cycle of refinement included 138 variable parameters and converged (largest parameter shift was 0.12 times its esd) with unweighted and weighted agreement factors of

$$R = \sum||F_o| - |F_c||/\sum|F_o|$$

$$R_w = \{\sum w(|F_o| - |F_c|)^2/\sum w|F_o|^2\}^{1/2}$$

The standard deviation of an observation of unit weight was 0.67. There were no correction coefficients greater than the highest peak in the final difference map, which had a height of 0.52 e/Å3 with an estimated error based on F[23] of 0.13. All calculations were performed on a VAX computer using SDP/VAX.[24] Figures were generated by using SHELXTL-PLUS (Nicolet Instrument Corp., Madison, WI, 1987.)

Generation of ZnSe, CdS, CdSe, and PbS Q Particles in Layered Phosphate and Phosphonate Hosts. The general procedure for producing II–VI binary semiconductor Q particles in the interlamellar region of zirconium phosphate and phosphonate is outlined as follows: The lattice water coordinated to Zn^{2+}, Cd^{2+}, or Pb^{2+} in $M^{II}[Zr(O_3PCH_2CH_2CO_2)_2]\cdot xH_2O$ (M = Zn, Cd, or Pb) and $M^{II}[Zr(PO_4)_2]\cdot yH_2O$ (M = Cd) was first removed by heating under vacuum at 240–260 °C for 24 h. This temperature is higher, by at least 20 °C, than that required for complete dehydration under ambient pressure, as determined by TGA. Dehydration does not alter the crystallinity of the solids significantly. After dehydration the samples were exposed to 1 atm of H_2S or H_2Se for at least 3 days. These gases were obtained from commercial sources (H_2S, Matheson, 99.5%; H_2Se, Alfagaz (Edison, NJ), 99.3%), used without purification, and introduced to the samples directly on a vacuum line. After the removal of the excess H_2S or H_2Se by evacuation for typically 2–3 days, samples were transferred to a drybox filled with argon, and the ensuing experiments were all performed with necessary precautions to avoid exposing samples to air.

Compound Analysis. The composition of semiconductors in the layered compounds was determined by atomic absorption spectroscopy (Galbraith, Knoxville, TN). X-ray powder diffraction (XRD) patterns were obtained with a Phillips diffractometer using monochromatized Cu Kα radiation. To prevent the moisture-sensitive samples from exposure to air, an airtight sample holder, which had an opening of arch shape that could be sealed with Scotch tape, was used. XRD revealed an interesting consequence of ion exchange for samples of $Zr(O_3PCH_2CH_2COOH)_2$ ($d_{interlayer}$ = 12.52 Å), $Na_2[Zr(O_3PCH_2CH_2COO)_2]\cdot zH_2O$ ($d_{interlayer}$ = 14.35 Å), and $Cd[Zr(O_3PCH_2CH_2CO_2)_2]\cdot xH_2O$ ($d_{interlayer}$ = 14.79 Å), i.e., that the intensity ratios of 002 reflection to 001 reflection ($d_{interlayer}$ is now taken as d_{001}) were 0.5, 2.0, and 100, respectively, for the three compounds. Steady-state fluorescence spectra were taken on a SPEX Florolog 2 fluorimeter. Transmission electron microscopy (TEM) experiments were performed with a JEOL 200 CX transmission electron microscope equipped with a LaB_6 emitter and a side-entry goniometer pole piece. Samples were dispersed in methanol and dropped as a slurry onto a holey carbon film supported by a Cu mesh. The holey carbon film had been coated with a thin film of Au as the internal standard for electron diffraction analysis. The methanol was allowed to evaporate leaving particles randomly distributed over the holey carbon film.

UV–vis diffuse-reflectance spectra were obtained with a Varian DMS 300 spectrophotometer equipped with diffuse-reflectance attachment, and the spectra were referenced to the acid form of zirconium phosphate or phosphonate, since the reaction producing the semiconductor particles was assumed to be as follows (⊃ denotes inclusion):

$$M^{II}[Zr(O_3PCH_2CH_2CO_2)_2] \text{ or } M^{II}[Zr(PO_4)_2] + H_2S \text{ or } H_2Se \Rightarrow M^{II}S \text{ or } M^{II}Se \supset Zr(O_3PCH_2CH_2CO_2H)_2 \text{ or } Zr(HPO_4)_2$$

Results and Discussion

Structure of $Zn[Zn(O_3PCH_2CH_2CO_2)]_2\cdot 3H_2O$. As the formula implies, there are two kinds of zinc atoms in this structure. In contrast to the slightly distorted octahedral coordination around zinc atom by oxygen atoms in the orthorhombic $Zn(O_3PR)\cdot H_2O$,[25] one of the zinc atoms is four-coordinated by oxygen atoms of the phosphonate

(19) *CAD4 Operations Manual*; Enraf-Nonius: Delft, Holland, 1977.
(20) Cromer, D. T.; Weber, J. T. *International Tables for X-ray Crystallography*, The Kynoch Press: Birmingham, England, 1974; Vol. IV, Table 2.2B.
(21) Ibers, J. A.; Hamilton, W. C. *Acta Crystallogr.* **1964**, *17*, 781.
(22) Cromer, D. T. *International Tables for X-ray Crystallography*; The Kynoch Press: Birmingham, England, 1974; Vol. IV, Table 2.3.1.
(23) Cruickshank, D. W. J. *Acta Crystallogr.* **1949**, *2*, 154.
(24) Frenz, B. A. The Enraf-Nonius CAD4 SDP—A Real-time System for Concurrent X-ray Data Collection and Crystal Structure Determination. In *Computing and Crystallography*; Schenk, H., Olthof-Hazelkamp, R., vanKonigsvel, H., Bassi, G. C., Eds.; Delft University Press: Delft, Holland, 1978; pp 64–71.
(25) Martin, K.; Squattrito, P. J.; Clearfield, A. *Inorg. Chim. Acta* **1989**, *155*, 7.

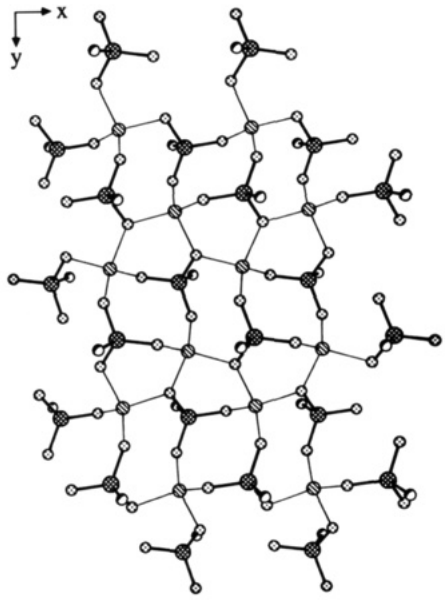

Figure 1. View down the *c* axis showing the coordination of Zn(1) by oxygen atoms of the phosphonate groups in $Zn[Zn(O_3PCH_2CH_2CO_2)]_2 \cdot 3H_2O$. H and C atoms not linked to phosphorus are omitted.

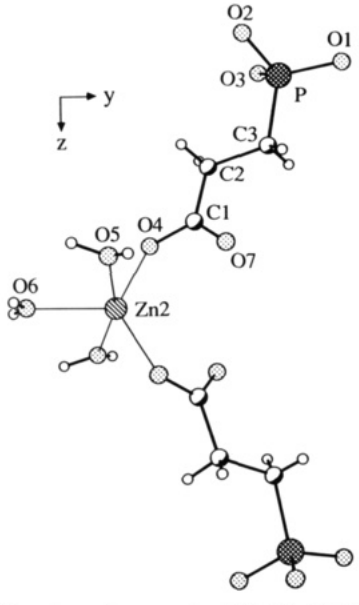

Figure 2. View down the *a* axis of $Zn[Zn(O_3PCH_2CH_2CO_2)]_2 \cdot 3H_2O$ showing the coordination of Zn(2) by two carboxylate oxygens and three water molecules.

groups (Figure 1), and the other is five-coordinated by two oxygen atoms of two carboxyl groups and three oxygen atoms of the lattice water molecules (Figure 2). The structure is a layered one, the repeating structure unit along the layering direction (*c* axis) is $Zn/O_3PCH_2CH_2CO_2/Zn(H_2O)_3/O_2CCH_2CH_2PO_3/$ as shown in Figure 3. There are two kinds of two-dimensional networks within each of the repeating units: one being zinc atoms linked by phosphonate oxygen atoms, and the other being a much weaker hydrogen bonding network linking the five-coordinated zinc atoms. A 2-fold axis runs through the bond between the zinc atom at the center of the oxygen trigonal bipyramid and the water molecule in the equatorial position. Positional and thermal parameters, bond lengths, and bond angles are listed in Tables I–III.

The positions of the water molecules in this structure account for the small decrease in layer distance of this

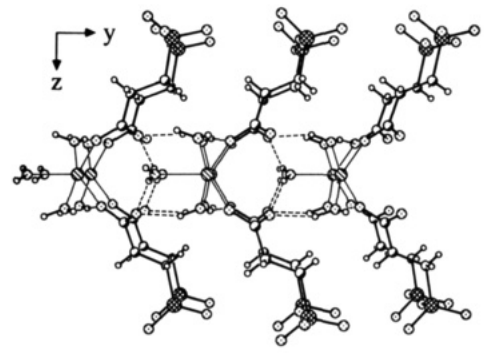

Figure 3. View down the *a* axis of $Zn[Zn(O_3PCH_2CH_2CO_2)]_2 \cdot 3H_2O$ showing the hydrogen-bonding network in the Zn(2)–carboxylate layer.

Table I. Positional and Equivalent Isotropic Thermal Parameters and Their Estimated Standard Deviations for $Zn[Zn(O_3PCH_2CH_2CO_2)]_2 \cdot 3H_2O$

atom	*x*	*y*	*z*	B_{iso}[a]
Zn1	0.20838 (9)	0.14886 (4)	−0.00131 (2)	0.923 (6)
Zn2	0.000	0.53486 (6)	0.250	1.14 (1)
P	0.2194 (2)	0.39877 (9)	0.05807 (3)	0.80 (1)
O1	0.3167 (7)	0.5267 (3)	0.0461 (1)	1.52 (5)
O2	0.3599 (5)	0.3037 (3)	0.0255 (1)	1.01 (5)
O3	0.4271 (6)	0.1207 (3)	−0.0546 (1)	1.61 (5)
O4	0.7807 (7)	0.3833 (3)	−0.2026 (1)	1.51 (5)
O5	0.2994 (7)	0.4940 (3)	−0.2016 (1)	2.20 (6)
O6	−0.500	0.1567 (4)	−0.250	2.65 (9)
O7	0.0825 (7)	0.2379 (3)	−0.1938 (1)	1.95 (6)
C1	0.8803 (9)	0.2916 (4)	−0.1804 (1)	1.24 (7)
C2	0.743 (1)	0.2553 (4)	−0.1359 (2)	1.86 (8)
C3	0.8246 (9)	0.1308 (4)	−0.1168 (1)	1.21 (6)
H6	0.83 (1)	0.316 (5)	0.241 (2)	1 (1)*
H21	0.56 (1)	0.263 (6)	−0.132 (2)	1 (1)*
H22	0.78 (1)	0.318 (5)	−0.117 (2)	0 (1)*
H31	0.26 (1)	0.423 (5)	0.133 (2)	0 (1)*
H32	0.06 (1)	0.123 (6)	−0.119 (2)	2 (2)*
H51	0.67 (1)	0.431 (5)	0.191 (2)	0 (1)*
H52	−0.12 (1)	0.042 (5)	0.198 (2)	0 (1)*

[a] Stars indicate isotropic refinement. Anisotropically refined atoms are given in the form of the isotropic equivalent displacement parameter defined as $^4/_3[a^2B(1,1) + b^2B(2,2) + c^2B(3,3) + ab(\cos\gamma)B(1,2) + ac(\cos\beta)B(1,3) + bc(\cos\alpha)B(2,3)$.

Table II. Bond Distances (Å) for $Zn[Zn(O_3PCH_2CH_2CO_2)]_2 \cdot 3H_2O$

Zn1	O1	1.899 (3)	O4	C1	1.284 (5)
Zn1	O2	2.002 (3)	O5	H51	0.89 *5)
Zn1	O2	1.984 (3)	O5	H52	0.57 (6)
Zn1	O3	1.916 (3)	O6	H6	0.95 (6)
An2	O4	1.973 (3)	O7	C1	1.250 (5)
Zn2	O4	1.973 (3)	C1	C2	1.508 (6)
Zn2	O5	2.091 (4)	C2	C3	1.515 (6)
Zn2	O6	2.076 (4)	C2	H21	0.95 (6)
P	O1	1.513 (3)	C2	H22	0.89 (5)
P	O2	1.564 (3)	C3	H31	0.82 (5)
P	O3	1.517 (3)	C3	H32	1.20 (7)
P	C3	1.792 (4)			

compound upon complete dehydration (28.6–28.0 Å). This small change suggests that after dehydration, the structure is rather open and may allow small gas molecules to diffuse in readily. This is important if semiconductor particles are to be produced within the interlamellar space. This structure is presumed to be related to that of $M^{II}[Zr(O_3PCH_2CH_2CO_2)_2] \cdot xH_2O$, in that the metal atoms involved in the formation of two-dimensional network are in the anhydrous layer, and the metal atoms coordinated by carboxyl groups are hydrated. In the absence of direct structural information on ion-exchanged $M^{II}[Zr(O_3PCH_2CH_2CO_2)_2] \cdot xH_2O$, the structure of $Zn[Zn(O_3PCH_2CH_2CO_2)]_2 \cdot 3H_2O$ serves as an aid for understanding the

Table III. Bond Angles (deg) for $Zn[Zn(O_3PCH_2CH_2CO_2)]_2 \cdot 3H_2O$

O1	Zn1	O2	109.7 (1)	O2	P	O3	108.9 (2)	O4	C1	C2	115.6 (4)
O1	Zn1	O2	111.6 (1)	O2	P	C3	107.5 (2)	O7	C1	C2	121.7 (3)
O1	Zn1	O3	119.8 (1)	O3	P	C3	109.5 (1)	C1	C2	C3	114.0 (3)
O2	Zn1	O2	105.4 (1)	Zn1	O1	P	141.1 (2)	C1	C2	H21	122 (4)
O2	Zn1	O3	102.2 (1)	Zn1	O2	Zn1	115.7 (1)	C1	C2	H22	101 (3)
O2	Zn1	O3	106.9 (1)	Zn1	O2	P	127.0 (2)	C3	C2	H21	108 (4)
O4	Zn2	O4	126.6 (1)	Zn1	O2	P	116.9 (2)	C3	C2	H22	114 (3)
O4	Zn2	O5	91.7 (1)	Zn1	O3	P	130.7 (1)	H21	C2	H22	96 (5)
O4	Zn2	O5	96.0 (1)	Zn2	O4	C1	117.4 (3)	P	C3	C2	114.4 (3)
O4	Zn2	O6	116.72 (8)	Zn2	O5	H51	121 (4)	P	C3	H31	106 (4)
O5	Zn2	O5	162.8 (2)	Zn2	O5	H52	121 (5)	P	C3	H32	110 (3)
O5	Zn2	O6	81.39 (8)	H51	O5	H52	116 (7)	C2	C3	H31	108 (4)
O1	P	O2	108.5 (2)	Zn2	O6	H6	108 (3)	C2	C3	H32	109 (3)
O1	P	P3	116.0 (2)	H6	O6	H6	143 (5)	H31	C3	H32	110 (5)
O1	P	C3	106.1 (2)	O4	C1	O7	122.6 (3)				

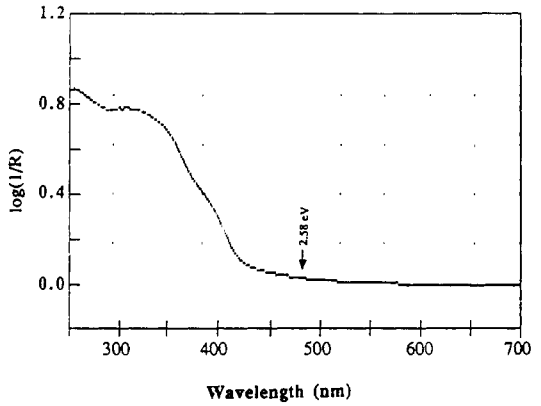

Figure 4. Diffuse-reflectance spectrum of $ZnSe_{0.62} \supset Zr(O_3PCH_2CH_2CO_2H)_2$. The arrow indicates the bandgap of bulk ZnSe.

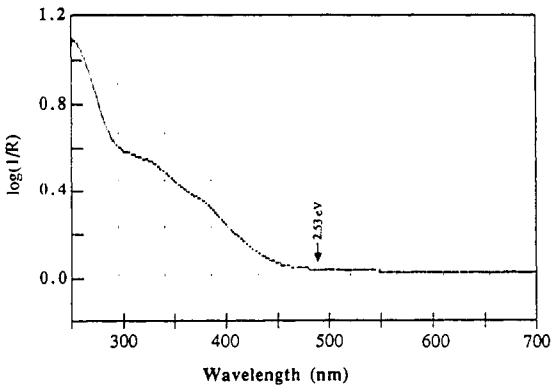

Figure 5. Diffuse-reflectance spectrum of $CdS_{0.73} \supset Zr(O_3PCH_2CH_2CO_2H)_2$. The arrow indicates the bandgap of bulk CdS.

chemical reactivity of $M^{II}[Zr(O_3PCH_2CH_2CO_2)_2]$ toward H_2Se and H_2S.

Reactivity of $Zn[Zn(O_3PCH_2CH_2CO_2)]_2 \cdot 3H_2O$, $M^{II}[Zr(O_3PCH_2CH_2CO_2)_2]$, and $M^{II}[Zr(PO_4)_2]$ toward H_2S or H_2Se. $Zn[Zn(O_3PCH_2CH_2CO_2)]_2 \cdot 3H_2O$, when dehydrated, reacts with H_2Se, affording a product, amorphous to X-rays, with an absorption onset corresponding to the bulk bandgap of ZnSe (2.58 eV). When samples of $M^{II}[Zr(O_3PCH_2CH_2CO_2)_2]$ (M = Zn, Cd, and Pb) were exposed to H_2Se or H_2S, the samples changed from white to pale yellow for ZnSe and CdS, to first bright yellow and then orange for CdSe, and to deep red for PbS. The reaction is rather slow, and it was consistently observed that $M^{II}[Zr(O_3PCH_2CH_2CO_2)_2]$ reacts slower with H_2Se than with H_2S. This result suggests that the reaction rate is controlled by solid-state diffusion of a chalcogen-containing species such as H_2X, $M(HX)_2$, or $(MX)_n$ (X = S, Se) and not by diffusion of M^{2+}. $Cd[Zr(O_3PCH_2CH_2CO_2)_2]$, after reacting 3 days with H_2S, afforded a product of stoichiometry of $CdS_{0.73}$, while H_2Se under the same conditions reached a stoichiometry of only $CdSe_{0.51}$. However, prolonged exposure (2 weeks) to H_2S or H_2Se gave a 1/1 metal/chalcogen ratio. The samples that gave spectra shown in Figures 4–7 had the stoichiometry $ZnSe_{0.62}$ (3-day reaction), $CdS_{0.73}$ (3-day reaction), $PbS_{0.80}$ (3-day reaction), and $CdSe_{1.05}$ (14-day reaction).

Attempts to prepare smaller semiconductor particles in $M^{II}[Zr(O_3PCH_2CH_2CO_2)_2]$ by exchanging inert ions[10] such as Ca^{2+} along with semiconductor precursor ions such as Cd^{2+} were not successful. When small amounts of Ca^{2+}

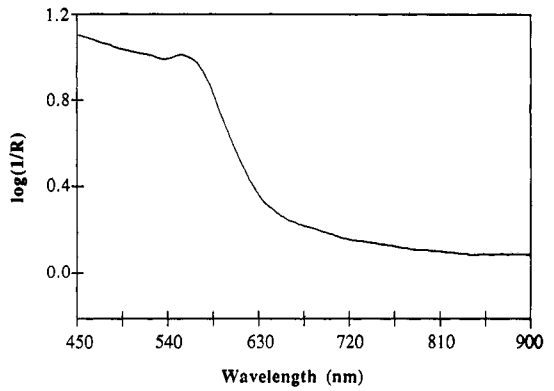

Figure 6. Diffuse-reflectance spectrum of $PbS_{0.80} \supset Zr(O_3PCH_2CH_2CO_2H)_2$.

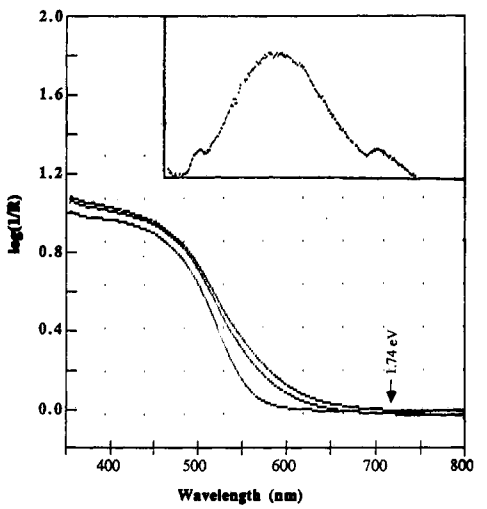

Figure 7. Diffuse-reflectance spectrum of CdSe $\supset Zr(O_3PCH_2CH_2CO_2H)_2$. Also shown is the spectral change when the sample is exposed to the moisture in air. From bottom up: no air, 1 h in air, and 4.5 h in air. Further exposure does not cause any more changes. The arrow indicates the bandgap of bulk CdSe. The inset is the emission spectrum taken from the no-air sample at 25 °C. λ_{ex} = 450 nm. The wavelength scale for the emission spectrum is the same as for the diffuse-reflectance spectrum.

were ion-exchanged into these materials, the formation of semiconductor, monitored by UV–visible spectral changes, is slowed dramatically. Particles grown under these conditions do not show quantum size effects, which suggests that they are formed on the external surface of the host crystals.

Figures 4–7 show diffuse-reflectance UV–visible spectra of ZnSe, CdS, PbS, and CdSe ⊃ $Zr(O_3PCH_2CH_2CO_2H)_2$. The absorption thresholds of the bulk materials are also indicated (at room temperature the bandgap is 2.58 eV for ZnSe, 1.74 eV for CdSe,[26a] 2.53 eV for CdS,[26b] and 0.41 eV for PbS[9b]). Note in Figure 6 that the absorption spectrum of PbS ⊃ $Zr(O_3PCH_2CH_2CO_2H)_2$ extends beyond 900 nm. Attempts to determine the absorption onset by taking the absorption spectrum of the powder sample embedded in polystyrene or poly(vinyl alcohol) on a quartz slide, using Varian Cary 2300 spectrophotometer with near-infrared capability, failed due to the very weak and gradual absorption tail and scattering from the sample. It is nevertheless certain that there was little absorption beyond 1500 nm, which corresponds to a bandgap of at least 0.83 eV. The emission spectrum of the CdSe sample (λ_{ex} = 450 nm) is shown in Figure 7. These samples were slightly sensitive to moisture, changing color very slowly when exposed to humid Texas air, as shown in Figure 7. However, the red shift of the absorption onset never reached that of the bulk semiconductor with prolonged exposure to air. Samples of CdS ⊃ $Zr(O_3PCH_2CH_2CO_2H)_2$ also display a blue-shift from the bulk absorption threshold, although less pronounced; however the absorption features in the higher energy region may indicate the existence of smaller Q particles. In contrast to these results, $M^{II}Zr(PO_4)_2$ (M = Cd) showed virtually no reactivity toward either H_2S or H_2Se. There was just a little color change upon introduction of H_2S or H_2Se to the solid sample, and the diffuse-reflectance spectra showed weak absorption with no blue shift with respect to the absorption edge of bulk CdS (517 nm) or CdSe (712 nm). This most likely indicates the formation of small amounts of bulklike particles on the external surface of the samples.

The difference in reactivity between $M^{II}[Zr(O_3PCH_2CH_2CO_2)_2]$ and $M^{II}[Zr(PO_4)_2]$ toward H_2S or H_2Se may be explained in terms of the accessibility of H_2S or H_2Se to the divalent metal ions in the layered structures. Since the dehydration of $M^{II}[Zr(O_3PCH_2CH_2CO_2)_2]\cdot xH_2O$ (M = Cd, for example) causes little change in interlayer spacing (14.79 (5) to 14.84 (5) Å) but the dehydration of $M^{II}[Zr(PO_4)_2]\cdot yH_2O$ (M = Cd) results in a large decrease in interlayer distance (from 9.50 to 7.91 Å, compared to 7.60 Å for $Zr(HPO_4)_2\cdot H_2O$), the accessibility of H_2S or H_2Se molecules to the divalent metal ions is obviously greater in $M^{II}[Zr(O_3PCH_2CH_2CO_2)_2]$ than in $M^{II}[Zr(PO_4)_2]$. Similar steric effects limiting the formation of Q-state semiconductor particles were reported for the formation of CdS particles in clays suspended in various solvents.[13a] Depending upon the molecular dimensions of the solvent molecule, which penetrates into the interlamellar region, different solvent molecules open up the clay layers to different extents, giving rise to the dependence of particle formation (either fast formation of Q particles or slow formation of bulk particles) on the solvents used.

Size of Q Particles. Two independent and complementary techniques, X-ray diffraction and transmission electron microscopy (TEM), were used to determine the particle size of the semiconductors formed from $M^{II}[Zr(O_3PCH_2CH_2CO_2)_2]$. Sample CdSe ⊃ $Zr(O_3PCH_2CH_2CO_2H)_2$ showed several extremely weak X-ray diffraction peaks corresponding to the layer distance (12.5 Å) of the host $Zr(O_3PCH_2CH_2CO_2H)_2$ and two similarly weak diffractions at 3.51 and 2.15 Å, attributable to the (111) and (220) diffractions of cubic CdSe, respectively. From the width of these diffraction peaks, the particle diameter of CdSe is calculated to be 45 (3) Å by using the Scherrer equation:[31] $D = k\lambda/B\cos\theta$, where D is the particle diameter, λ is the X-ray wavelength, B is the half-width of the diffraction peak corrected for peak width due to the instrument, θ is the diffraction angle, and k is a constant taken to be 1. This size correlates well with the optical bandgap of the CdSe Q particles, which can be determined on the basis of the following relation for direct bandgap semiconductors:[27]

$$\alpha \propto (h\nu - E_g)^{1/2} \quad (1)$$

where α is the absorption coefficient, $h\nu$ is the photon energy, and E_g is the bandgap. The absorption coefficient α is related to reflectance R by

$$\alpha = SF(R)/2\nu_p \quad (2)$$

where S is the scattering coefficient, ν_p is the volume fraction of the absorbing species, and $F(R)$ is Kubelka–Munk function:[28]

$$F(R) = (1 - R)^2/2R \quad (3)$$

in which R is the experimentally observed reflectance. If the dependence of the scattering coefficient S on wavelength of the incident light is neglected, the Kubelka–Munk function is directly proportional to the absorption coefficient α:

$$\alpha = (S/2\nu_p)F(R) = \text{constant} \times F(R) \quad (4)$$

Therefore for the purpose of determining the bandgap, extrapolating the $F(R)^2$ vs energy curve to $F(R)^2 = 0$ is equivalent to carrying out the same procedure with the α^2 vs energy curve. Shown in Figure 8 is a plot of $F(R)^2$ vs photon energy. The bandgap for CdSe ⊃ $Zr(O_3PCH_2CH_2CO_2H)_2$ is determined to be 2.40 eV, 0.66 eV larger than the bandgap of bulk CdSe. (It should be noted that, strictly, the scattering coefficient S is not independent of wavelength of the incident light when the particle size of a solid sample is comparable to the wavelength of incident light.) Comparison of this bandgap change to that reported in the literature[29] for well-characterized "phenyl-capped"

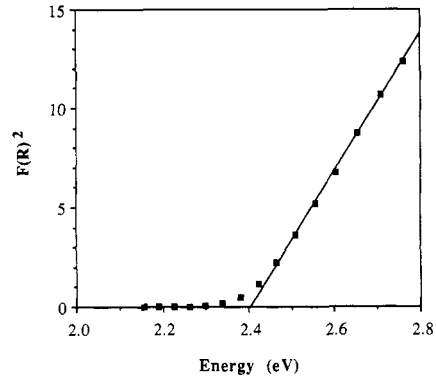

Figure 8. Plot of $F(R)^2$ vs photon energy for Q–CdSe included in $Zr(O_3PCH_2CH_2CO_2H)_2$. The intercept 2.40 eV at $F(R)^2 = 0$ is the bandgap.

(26) (a) Chestnoy, N.; Brus, L. E. *J. Chem. Phys.* **1986**, *85*(4), 2237. (b) Rossetti, R.; Hull, R.; Gibson, J. M.; Brus, L. E. *J. Chem. Phys.* **1985**, 1406.

(27) Moss. T. S. *Optical Properties of Semiconductors*; Academic Press: New York, 1959.

(28) *Reflectance Spectroscopy*; Kortum, G., Ed.; Springer-Verlag: New York, 1969.

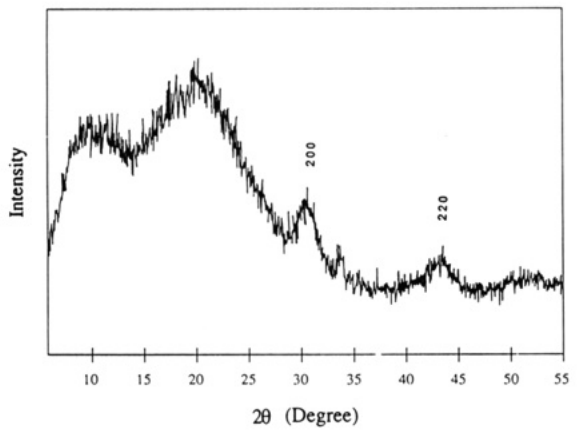

Figure 9. X-ray powder diffraction pattern of $PbS_{0.80} \supset Zr(O_3PCH_2CH_2CO_2H)_2$. One of the strongest reflections of PbS, the 200 reflection, is under the broad diffraction maxima of the amorphous Scotch tape, which was used to cover the opening of the sample holder for protection against moisture in air.

CdSe gives an estimate of 40–45 Å for the diameter of CdSe ⊃ $Zr(O_3PCH_2CH_2CO_2H)_2$ if the particles are considered spherical.

In principle the above procedure could be carried out for all the semiconductor Q particles prepared. Difficulties were encountered in doing so because the diffuse-reflectance spectra of ZnSe, CdS, and PbS ⊃ $Zr(O_3PCH_2CH_2CO_2H)_2$ (Figures 4–6, respectively) were not as simple as that of CdSe ⊃ $Zr(O_3PCH_2CH_2CO_2H)_2$, and the powder diffraction patterns of ZnSe and CdS ⊃ $Zr(O_3PCH_2CH_2CO_2H)_2$ show no reflections that could be attributed to the semiconductors, possibly due to the weaker scattering element involved. Therefore the bandgaps of these Q particles were estimated from their absorption edges. The absorption edge of ZnSe ⊃ $Zr(O_3PCH_2CH_2CO_2H)_2$ is at about 430 nm (Figure 4). This corresponds to bandgap of 2.88 eV, which is 0.30 eV larger than the bandgap of bulk ZnSe.[26a] This bandgap energy is comparable to that previously observed with colloidal suspensions of 40–50-Å diameter ZnSe Q particles, which had an absorption onset of ca. 420 nm (−80 °C).[26a,30] Likewise, CdS ⊃ $Zr(O_3PCH_2CH_2CO_2H)_2$ has an absorption onset at 450 nm (Figure 5). This corresponds to 2.76 eV, 0.23 eV larger than the bandgap of bulk CdS. The corresponding diameter of these CdS particles is estimated to be about 50 Å.[26b]

In the case of PbS ⊃ $Zr(O_3PCH_2CH_2CO_2H)_2$, the bandgap is at least 0.83 eV, as indicated above. The X-ray diffraction pattern showed the (111), (200), and (220) reflections of PbS with the rocksalt structure (Figure 9). From the peak width, a particle diameter of 38 (3) Å was calculated by using Scherrer's equation. By comparison with the PbS Q particles generated in ethylene–methacrylic acid copolymer,[9] PbS particles of 38-Å diameter should have a bandgap of 1.2 ± 0.1 eV.

Electron Microscopic Study of the Q Particles. CdSe ⊃ $Zr(O_3PCH_2CH_2CO_2H)_2$. The overall appearance of the sample is that of the thin hexagonal platelets of the host compound $Zr(O_3PCH_2CH_2CO_2H)_2$. Bright field images of very thin platelet show uniformly distributed patches of greater projected mass, ca. 40–50 Å in diameter, throughout the 300–500-Å-thick plates (Figure 10). Although the host material appears, from the image, to retain its structure, electron diffraction with the electron beam directed perpendicular to the thin plates showed only the (111), (220), and symmetry-equivalent reflections of CdSe in the zinc blende structure (Figure 11) and no diffraction peaks from the host. Surprisingly, these broad diffraction maxima from the CdSe show 6-fold symmetry, indicative of ordering of CdSe crystallites within the disordered host (vide infra). The absence of reflections from the host in the [001] zone electron diffraction is consistent with the XRD observation that CdSe ⊃ $Zr(O_3PCH_2CH_2CO_2H)_2$ showed only extremely weak reflections from the host basal plane. Attempts to image the diffracting CdSe using dark-field techniques were unsuccessful because of the weak diffraction and problems of sample shrinking and drifting under the electron beam, perhaps due to thermal expansion and damage by the electron beam.

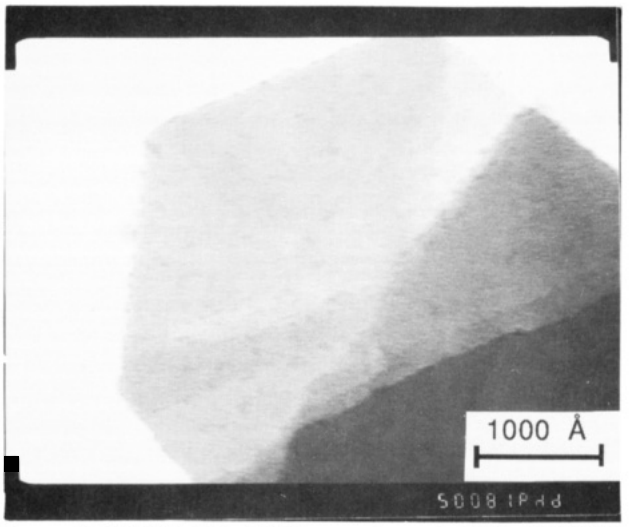

Figure 10. TEM bright-field image of sample CdSe ⊃ $Zr(O_3PCH_2CH_2CO_2H)_2$.

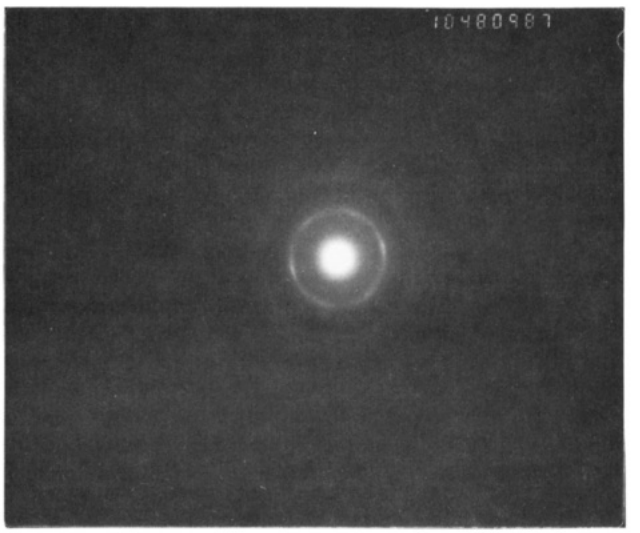

Figure 11. Electron diffraction pattern taken with the electron beam directed perpendicular to the platelet of sample CdSe ⊃ $Zr(O_3PCH_2CH_2CO_2H)_2$.

The electron diffraction pattern in Figure 11 suggests that the CdSe particles that gave rise to the observed reflections not only are oriented with their [111] zone axis perpendicular to the host layer plane but also are aligned with each other, giving rise to the 6-fold spot diffraction pattern. This may be an example of lattice-controlled crystal growth. First, the layered host lattice will certainly encourage the growth of a foreign crystal within it to be

(29) Steigerwald, M. L.; Alivisatos, A. P.; Gibson, J. M.; Harris, T. D.; Kortan, R.: Muller, A. J.; Thayer, A. M.; Duncan, T. M.; Douglass, D. C.; Brus, L. E. *J. Am. Chem. Soc.* **1988**, *110*, 3046.
(30) Nedeljkovic, J. M.; Nenadovic, M. T.; Micic, O. I.; Nozik, A. J. *J. Phys. Chem.* **1986**, *90*, 12.
(31) Azaroff, L. V. *Elements of X-ray Crystallography*; McGraw-Hill: New York, 1968; p 552.

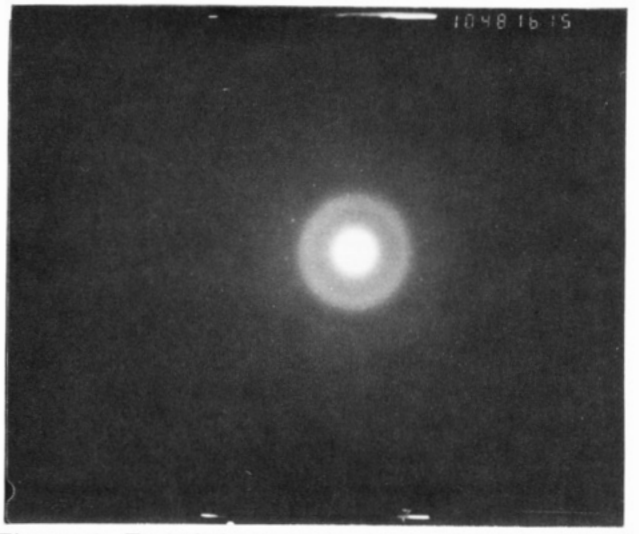

Figure 12. Typical electron diffraction pattern taken from a platelet of the sample $PbS_{0.80} \supset Zr(O_3PCH_2CH_2CO_2H)_2$. The diffraction spots are from Au internal standard.

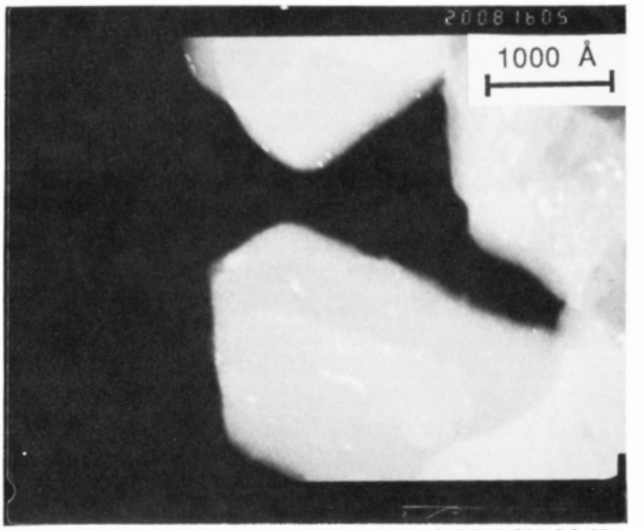

Figure 13. Dark-field image of $PbS_{0.80} \supset Zr(O_3PCH_2CH_2CO_2H)_2$.

anisotropic. Therefore it is not surprising to find that the [111] direction, which is the direction of alternating layers of Cd and Se atoms in the zinc blende structure, is perpendicular to the layer plane of the host. This aspect of lattice control by the host must be in effect as long as the host retains its layer ordering, which was found to be the case after the Q-particle formation. In addition, the alignment of CdSe particles relative to one another can originate only in the early stages of CdSe formation when the host compound is still crystalline. One may postulate the process as follows: at the beginning when nuclei of CdSe are just formed inside the ordered, layered crystalline lattice of $Cd[Zr(O_3PCH_2CH_2CO_2)_2]$, they are oriented in the plane of the host pseudohexagonal lattice. As the CdSe particles grow bigger, the crystallinity of the host lattice is destroyed, but in the meantime the particles have already grown big enough so that in-plane rotational motion relative to one another is hindered. Therefore the initial ordering of CdSe nuclei imposed by the host lattice is retained, resulting in the seemingly impossible ordering of a guest compound in a nearly amorphous host.

$PbS \supset Zr(O_3PCH_2CH_2CO_2H)_2$. The bright-field image of this sample shows small areas, ca. 30–40 Å in diameter, of greater projected mass amid the thin platelets of the host material. Electron diffraction from areas of the platelets showed reasonably well-defined diffraction rings corresponding to the (111), (002), and (220) reflections of cubic PbS (Figure 12) in the rocksalt structure, consistent with the XRD result. Dark-field images (Figure 13) indicate that the diffracting species are small (30–40 Å) PbS particles uniformly distributed throughout the platelets, as well as a few significantly larger PbS particles (100–400 Å) along the edges of the host platelets. These larger particles could be responsible for the observed weak absorption tail extending into the near-IR region.

Conclusions

We have shown in this study that Q-state semiconductors can be produced within the interlamellar region of a layered compound, if the host compound allows the access of H_2S or H_2Se to the precursor metal ions. These semiconductor particles show quantum size shifts in their electronic absorption spectra relative to bulk semiconductors. The correlation between the semiconductor particle size, determined by X-ray diffraction and/or TEM, and the magnitude of blue shift agree closely with the literature for well-characterized "capped" semiconductor particles. In all cases the diameter of the semiconductor particles produced within the layered $Zr(O_3PCH_2CH_2CO_2H)_2$ host is in the range 30–50 Å; particle size appears to be controlled by the restriction of mass transport during the growth of crystallites within the interlamellar region.

TEM experiments provide definitive evidence for the inclusion of the semiconductor Q-particles within platelets of $Zr(O_3PCH_2CH_2CO_2H)_2$ and give a direct determination of their size. Particles of PbS, ca. 30–40 Å in diameter, and particles of CdSe, 40–50 Å in diameter, are uniformly distributed in the layered host platelets. In the case of CdSe, electron diffraction shows ordering of CdSe particles, relative both to the host layers and among themselves. This is interpreted as a consequence of lattice controlled crystal growth.

Acknowledgment. This work was supported by grants from the National Science Foundation (PYI Award CHE-8657729) and by the Robert A. Welch Foundation. T.E.M. also thanks the Camille and Henry Dreyfus Foundation for support in the form of a Teacher–Scholar Award.

Registry No. $Na_2[Zr(O_3PCH_2CH_2CO_2)_2]$, 77849-49-1; $Zr(O_3PCH_2CH_2CO_2H)_2$, 75406-99-4; $Zn^{II}[Zr(O_3PCH_2CH_2CO_2)_2]$, 130147-22-7; $Pb^{II}[Zr(O_3PCH_2CH_2CO_2)_2]$, 130147-23-8; $Cd^{II}[Zr(O_3PCH_2CH_2CO_2)_2]$, 130147-24-9; $Zn[Zn(O_3PCH_2CH_2CO_2)]_2 \cdot 3H_2O$, 130147-25-0; $Cd[Zr(O_3PCH_2CH_2CO_2)_2] \cdot xH_2O$, 130147-26-1; $Cd[Zr(PO_4)_2] \cdot yH_2O$, 130147-20-5; $Na_2[Zr(O_3PCH_2CH_2CO_2)_2 \cdot zH_2O$, 130147-27-2; ZnSe, 1315-09-9; PbS, 1314-87-0; CdSe, 1306-24-7; CdS, 1306-23-6; $Cd^{II}[Zr(PO_4)_2]$, 130147-21-6; $Zn[Zn(O_3PCH_2CH_2CO_2)]_2$, 130147-28-3.

Supplementary Material Available: Tables S1 and S2, containing crystallographic data for $Zn[Zn(O_3PCH_2CH_2CO_2)]_2 \cdot 3H_2O$ and anisotropic thermal parameters for non-H atoms (3 pages); Table S3, listing observed and calculated structure factors (8 pages). Ordering information is given on any current masthead page.